Physica D 55 (1992) 368–384
North-Holland

PHYSICA D

Mean field fluctuation of a network of chaotic elements

Remaining fluctuation and correlation in the large size limit

Kunihiko Kaneko

Department of Pure and Applied Sciences, College of Arts and Sciences, University of Tokyo, Komaba, Meguro-ku, Tokyo 153, Japan

Received 21 May 1991
Revised manuscript received 23 November 1991
Accepted 26 November 1991
Communicated by A.V. Holden

Fluctuation of the mean field is studied for a network of chaotic elements with the use of globally coupled maps. As the size N is increased, the variance of the mean field decreases up to a crossover size N_c, but then stays constant, where the remaining variance is roughly proportional to $1/N_c$. The distribution of the mean field approaches a Gaussian form up to N_c, but keeps some deviation for $N > N_c$. The breakdown of the law of large numbers implies some hidden coherence among elements, confirmed by finite mutual information and Lyapunov spectra. The breakdown is also supported by the instability of the self-consistent solution for the Perron–Frobenius operator. The anomalous effect of additional noise to our system is also reported. Results from other globally coupled maps suggest that the law of large numbers is generally broken in a turbulent phase with local stretching and contraction, but is satisfied for a map with stretching only.

1. Introduction

Globally coupled dynamical systems are an important field in nonlinear dynamics. The dynamics is known to bring some novel notions; clustering, hierarchical structure, chaotic itinerancy, partition complexity and so on [1–3]. This class of dynamical systems is seen in broad branches of science [1, 4]. In physics, coupled nonlinear oscillators with a global feedback frequently occur in a Josephson junction array or a charge density wave with a constant electric current. In optics, many modes are often coupled globally through an energy source [5, 6][#1]. Other examples of long-ranged nonlinear coupling include vortex, galaxy, and protein dynamics.

Globally coupled dynamical systems are seen in evolutionary dynamics [7] and economics. They are also important in complex biological information processing. In neurodynamics, a single neuron and a small ensemble of neurons [8] are known to exhibit chaotic behavior. These ensembles of neurons are connected through a complex global coupling. So far, most of neural network studies take elements of trivial dynamics with a global coupling. Instead, it is also important to study a model with complex dynamical elements (with a chaotic response) and simple global couplings, as another limit of simplification of neurodynamics.

We have studied one of the simplest models among such globally coupled dynamical systems; a globally coupled map (GCM), originally introduced [1, 4] as a mean-field-type extension of coupled map lattices (CML) [9, 10]. GCM is a

[#1] The authors of ref. [6] find that the mean-field distribution for a multi-mode laser is rather close to a Gaussian one.

dynamical system with a discrete time whose elements interact with all other elements.

Here we focus on

$$x_{n+1}(i) = (1-\varepsilon) f(x_n(i)) + \frac{\varepsilon}{N} \sum_{j=1}^{N} f(x_n(j)), \tag{1}$$

where n is a discrete time step and i is the index of elements ($i = 1, 2, \ldots, N$ = system size) [1]. The mapping function $f(x)$ is chosen so that it can show one-dimensional chaos. Up to section 5 we use the logistic (quadratic) map

$$f(x) = 1 - ax^2, \tag{2}$$

since it has been investigated in detail as a prototype of dissipative chaos. Other examples are seen in later sections.

An important idea in globally coupled dynamical systems is *clustering*. After our system falls on an attractor, elements $x_n(i)$ split into k clusters, where all elements in the same cluster oscillate in synchronization. The clustering state is time-invariant once our system falls on an attractor. As has been studied earlier [1], there are four phases with different rates of clustering, ranging from coherent phase to a completely desynchronized phase [1] ($k = N$).

Our model has two conflicting tendencies; destruction of coherence by the chaotic instability of each element, and synchronization by global averaging. In the turbulent phase, the former tendency wins and none of elements are synchronized.

Earlier we have reported the breakdown of the law of large numbers and the emergence of subtle coherence [1]. Here we study the fluctuation of the mean field in detail. The present paper is organized as follows:

In section 2, the mean-field fluctuation is studied for globally coupled logistic maps. Up to a crossover size the variance of the mean-field distribution decreases with the size N but it remains finite even in the limit of $N \to \infty$. The distribution of the mean field approaches a Gaussian one up to N_c but keeps some deviation at its tail for $N > N_c$. The parameter dependence of the distribution form is studied in detail. The remaining fluctuation suggests some hidden coherence among elements, which is confirmed with the use of mutual information and Lyapunov spectra in section 3. The single-point distribution is time-dependent due to the remaining fluctuation. Indeed, numerical studies of the Perron–Frobenius operator suggest instability of the self-consistent solution of invariant measure. The effect of additional noise on our system is studied in section 4. When the noise amplitude is large, the variance of mean-field decreases with size, leading to the recovery of the law of large numbers. The decrease of variance and mutual information is fitted by $N^{-\beta}$, with the exponent β depending on the noise. Section 5 is devoted to a related problem; globally coupled quadratic maps with a distributed parameter depending on elements. This problem can be reduced to a globally coupled map with a static noise differing by elements. The mean field fluctuation decreases with size up to some size, but it comes back to the original noiseless level with the further increase of N.

In section 6, we have studied a globally coupled tent map. Contrary to the quadratic map case, the mean-field fluctuation obeys the law of large numbers and the central limit theorem in the turbulent phase. The mean field fluctuation of globally coupled circle maps is studied in section 7. The law of large numbers is satisfied in the torus phase, while the variance remains finite for $N \to \infty$ limit in the turbulent phase. For these three types of globally coupled maps, the law of large numbers is not satisfied in the turbulent phase with local stretching and contraction. Section 8 is devoted to summary and discussion.

2. Mean field fluctuation: breakdown of law of large numbers and central limit theorem

Our mean-field $(1/N)\Sigma_i f(x_n(i))$ fluctuates in time. In the turbulent phase, $x_n(i)$ takes almost random values almost independently. Then, one

might expect that the aggregate

$$h_n \equiv \frac{1}{N}\sum_j f(x_n(j)) \qquad (3)$$

obeys the law of large numbers. If this were the case, the mean square deviation (MSD) of the mean field h would decrease with N as N^{-1}. The interaction term in (1) could be replaced by a noise whose root mean square is $\mathcal{O}(1/\sqrt{N})$. Then, in the limit $N \to \infty$, the dynamics (1) would reduce to N independent logistic maps given by $x_{n+1}(i) = (1-\varepsilon)f(x_n(i)) + \varepsilon C$, where $C = (1/N)\Sigma_i f(x(i))$ is a constant mean field.

We have measured the distribution of the mean field h_n. Numerically, the distribution function $P(h)$ is rather close to a Gaussian form. The distribution sharpens with size up to some size, but the sharpening stops with the further increase of size (fig. 1). In fig. 1, note also that a distribution of a single point $x_n(i)$ is far from Gaussian, and keeps some singular feature of an invariant measure of a single logistic map. This distribution contrasts strongly with that for the mean field.

To examine the law of large numbers, we have plotted the mean square deviation (MSD) of the mean field (see fig. 2), $\langle(\delta h)^2\rangle \equiv \langle(h - \langle h\rangle)^2\rangle$, where $\langle \ldots \rangle$ is the average by the distribution $P(y)$; $\langle A\rangle \equiv \int P(h)\,A(h)\,dh$. If each element $x(i)$ were approximated by an uncorrelated random number, it is expected that $\langle(\delta h)^2\rangle \propto 1/N$ would hold. In fig. 2, the decrease of MSD with N is plotted for different values of a. In globally coupled chaos the law of large numbers is not valid.

To check the form of the distribution itself, we have measured the flatness of the system given by $\langle(h - \langle h\rangle)^4\rangle / [\langle(\delta h)^2\rangle]^2$, which should take the value 3 for a Gaussian distribution. The flatness is plotted as a function of size in fig. 3. As is seen, the flatness deviates from 3 in general for $N > N_c$, although the deviation is rather small for some parameter values of a. The distribution approaches a Gaussian form up to N_c and then deviates a little at the tail of its distribution. The

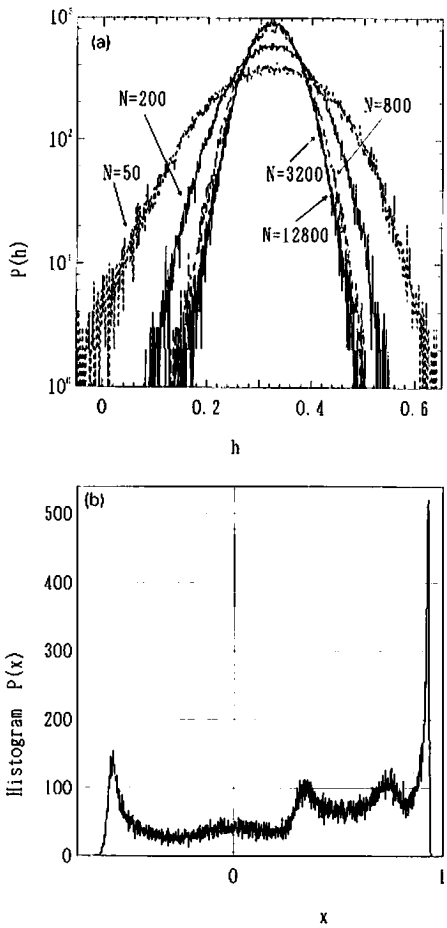

Fig. 1. (a) Semi-log plot of histogram of mean field h_n. Sampled over 10^5 time steps, after discarding initial 10^4 steps, using the bin width 10^{-3}. $a = 1.95$ and $\varepsilon = 0.1$. Sizes are $N = 50$ (broken line), 200, 800 (broken line), 3200, and 12800. Histograms for the last two sizes agree within a statistical error. (b) For comparison, distribution of a single point $x_n(i)$ is plotted for the same parameters with $N = 3200$.

central limit theorem is also quantitatively broken[#2].

There is no a priori reason why the distribution of mean field is symmetric about its peak. We have calculated $\langle(\delta h)^3\rangle$ numerically. The value is

[#2] Since the distribution here is bounded, the distribution cannot be exactly Gaussian at its tail. When the law of large numbers and the central limit theorem are satisfied, the Gaussian distribution is attained after the variance is scaled by $1/N$, where the distribution can be unbounded in the limit of $N \to \infty$.

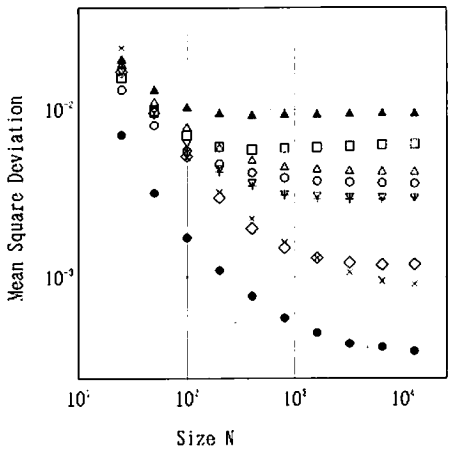

Fig. 2. Mean square deviation (MSD) of the distribution of mean field h_i plotted as a function of system size. The MSD is calculated over 10^5 time steps after 10^4 transients. $\varepsilon = 0.1$. The parameter a is 1.81 (●), 1.84 (○), 1.86 (□), 1.88 (◇), 1.91 (△), 1.94 (▲), 1.96 (▽) and 1.98 (x).

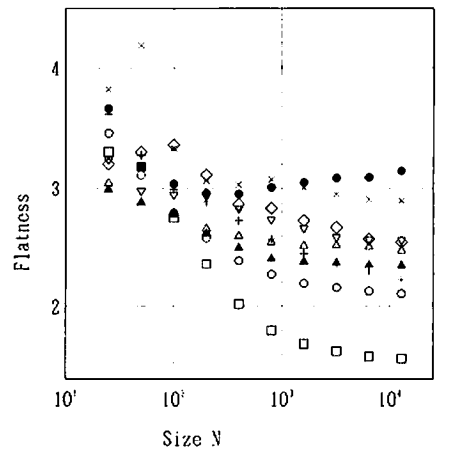

Fig. 3. Flatness of the mean-field distribution plotted as a function of size, corresponding to the data for fig. 2. Same notation for the parameter a as fig. 2.

close to zero within our accuracy. Symmetry is almost attained.

The parameter dependence of N_c and of the asymptotic MSD (for $N \to \infty$) on a is irregular, and may reflect the singular parameter dependence of chaos of a single logistic map (see fig. 4). This irregular behavior contrasts strongly with the smooth behavior of quantifiers of spatiotemporal chaos in short-ranged coupled map lattices [11].

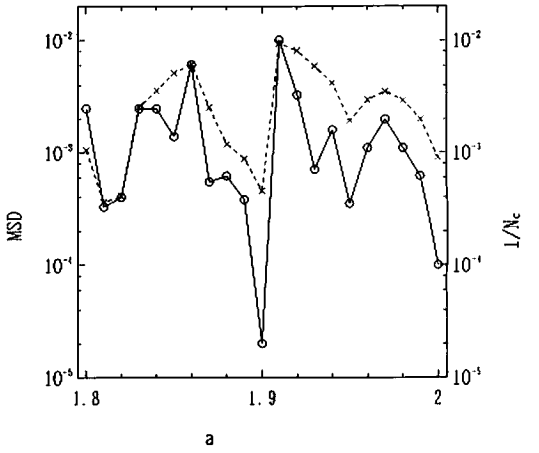

Fig. 4. Dependence of MSD and N_c on the parameter a for $\varepsilon = 0.1$. The asymptotic MSD (○) (for $N \gg N_c$) and $1/N_c$ (x) are plotted as a function of a. Both quantities are estimated from the graph corresponding to fig. 2 (The estimate of N_c is not necessarily accurate). Data are obtained from the mean-field distribution sampled over 10^5 time steps after discarding initial 10^4 transients.

Data for the asymptotic MSDs at $N \gg N_c$ suggest that N_c is roughly inversely proportional to the asymptotic MSD[#3]. Since MSD is in the same order at a small size for different parameters and decreases with $1/N$, this relation is expected.

In fig. 5 asymptotic flatness is plotted as a function of N_c. Roughly speaking, the asymptotic flatness is closer to three as N_c gets larger. Indeed, the distribution is rather close to a Gaussian form except at its tail for $a = 1.95$ and 2.0, where N_c is rather large. For parameters with smaller N_c, the approach to Gaussian form is not good.

Dependence on the coupling ε. In the limit of $\varepsilon \to 0$, it is expected that our system approaches N independent logistic maps, and that the mean field fluctuation obeys the law of large numbers. How do our MSD and N_c approach this limit as $\varepsilon \to 0$?

In fig. 6 we have plotted MSD as a function of size with the change of ε. The corresponding change of flatness is given in fig. 7. As ε goes to

[#3]Although the estimate of N_c is rather inaccurate here, this tendency of proportionality is seen in fig. 4.

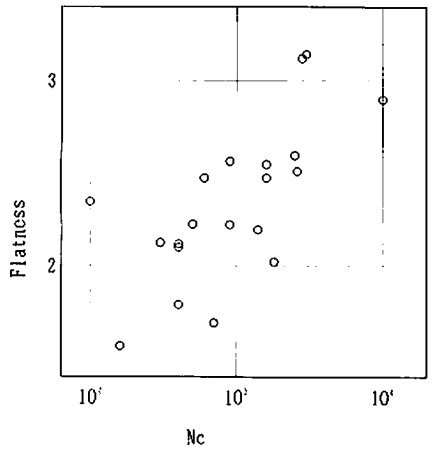

Fig. 5. Asymptotic flatness (for $N \gg N_c$) plotted as a function of N_c, obtained from the data for fig. 4.

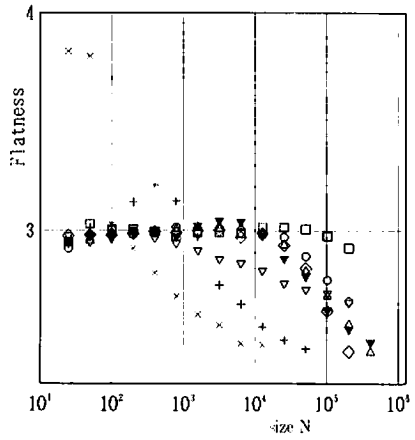

Fig. 7. Flatness corresponding to fig. 6 is plotted as a function of size. Notations are same as in fig. 6.

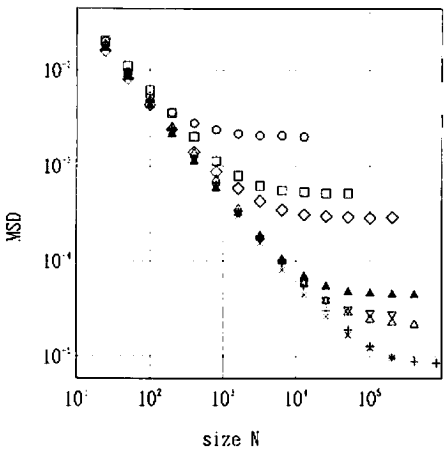

Fig. 6. Mean square deviation (MSD) of the distribution of mean field h_i plotted as a function of system size. The MSD is calculated over 10^5 time steps after 10^4 transients $a = 1.99$. The coupling ε is 0.1 (○), 0.05 (□), 0.03 (◇), 0.02 (▲), 0.01 (△), 0.009 (▽), 0.008 (+), and 0.005 (x).

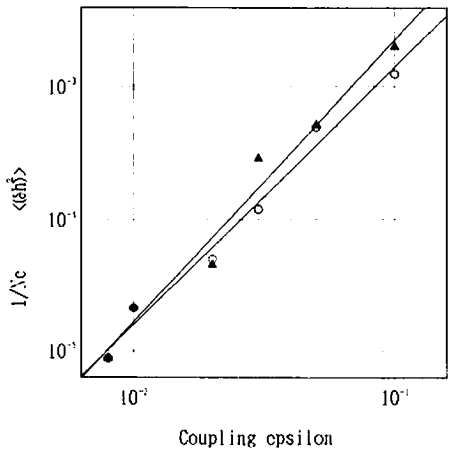

Fig. 8. Dependence of asymptotic MSD (▲) and $1/N_c$ (○) on the parameter ε. Both quantities are estimated from the data for fig. 6. (The estimate of N_c is not necessarily accurate). The least square fit in the figure has slopes 1.95 and 2.1, inconsistent with 2.0.

zero, the crossover size N_c increases. Up to $N \approx N_c$ the approach to a Guassian form is quite good especially if ε is small (see fig. 7). The asymptotic MSD is again inversely proportional to N_c. Their dependence on coupling ε is given in fig. 8. The data suggest[#4] the dependence of $\langle(\delta h)^2\rangle_\infty \propto 1/N_c \propto \varepsilon^2$.

[#4]There also exists non-monotonic dependence on ε besides the above square dependence.

3. Emergence of hidden coherence

Since the law of large numbers is a general property in a bounded uncorrelated random process, the existence of the size-independent fluctuation suggests a remaining correlation among elements. We measure the power spectrum for the mean field h_n through $|\Sigma_n h_n e^{inw}|^2$. The spectrum is continuous since the dynamics of the mean field is aperiodic. However, broad peaks

remain in the power spectrum. The peaks get sharper with further increase of size N up to N_c. For $N > N_c$, the spectrum is invariant against the increase of N. The sharpening suggests the emergence of a partly coherent motion. In the power spectrum of the timeseries $x_n(i)$ of a single element i, we have not seen such sharpening of peaks with the size.

To study the correlation among elements we have measured the mutual information among elements [12, 13]. The mutual information is calculated through a single point probability $P_i(y)$ that $x(i)$ takes y, and a two-point probability $p_{i,j}(y,z)$ that $x(i)$ takes y and $x(j)$ takes z $(i \neq j)$. These probability distributions are calculated from a long time sample. Mutual information $\mu_{i,j}$ is given by

$$-\iint p_{i,j}(x,y)\log\frac{p_{i,j}(x,y)}{P_i(x)P_j(y)}\,dx\,dy.$$

Since the distributions seem to be independent of sites i, the mutual information is also site-independent and the suffices in $\mu_{i,j}$ can be removed.

In fig. 9, we have plotted μ with the change of size N. As is seen, there remains a finite mutual correlation even if N gets large. In fig. 9, we have also plotted the mutual information for a system with noise (see section 4). A remaining finite mutual correlation in a noiseless system is clearly seen.

One might expect that the hidden coherence might be temporal in nature as in frozen order in the spin glass problem [14]. To check this possibility, we have measured the probability that two close elements stay closer with the time evolution. In practice, we have defined the following relative closeness $S_n^{i,j}$ between two elements introducing a precision δ to judge the closeness:

$$S_n^{i,j} = 1 \quad \text{if } |x_n(i) - x_n(j)| < \delta,$$
$$= 0 \quad \text{otherwise,}$$

The temporal correlation function given by $C(t) = \sum_{i,j}(\langle S_{m+t}^{i,j} S_m^{i,j}\rangle - \langle S_m^{i,j}\rangle^2)$ always decays

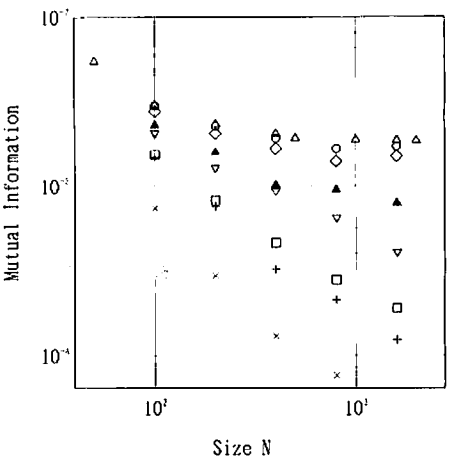

Fig. 9. Two-point mutual information. Calculated from $2\times 10^7/N$ time steps after discarding 10^4 transients. Noiseless case (△), and with random numbers homogeneously distributed over $[-\sigma,\sigma]$. $\sigma = 0.005$ (○), 0.0075 (◇), 0.002 (▲), 0.004 (▽), 0.005 (□), 0.01 (+), and 0.02 (x). $a = 1.99$ and $\varepsilon = 0.1$.

exponentially to zero with time for our turbulent state, unless the precision δ is too large (≈ 0.5). Thus our coherence is not a frozen relationship between two elements.

One may expect that the orbit uses more contraction parts to create coherence, as N is increased. In fig. 10, we have plotted a long-time histogram of the single point distribution $x_n(i)$ for $N \gg N_c$ subtracted by that for $N < N_c$. A shift of some broad peaks is seen. There is a slight shift in the direction of smaller $|f'(x)|$, which increases the measure at a contractive region. The distribution shift, however, includes more complicated structures, and it is rather difficult confirm the above tendency clearly. The origin of coherence is hidden in nature and is not easily revealed as yet.

Does the emergence of subtle coherence change the nature of chaos? To address this question we have computed Lyapunov spectra from the product of Jacobi matrices. Eigenvalues of the product, arranged in the decreasing order, form the spectrum [15]. Fig. 11 displays Lyapunov exponents λ_i for sizes 50, 100, 400, and 600. We plot λ_i as a function of scaled index i/N follow-

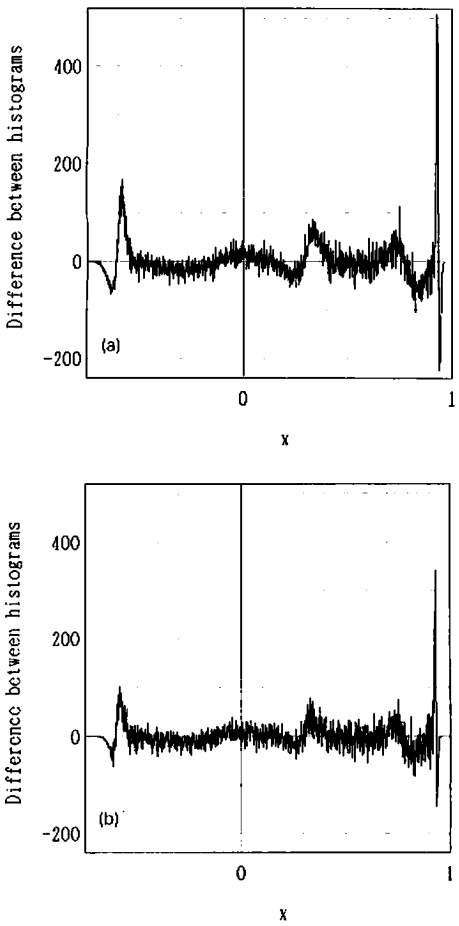

Fig. 10. Difference between histograms for distribution of a single point $x_n(i)$, sampled over 10^5 time steps, after discarding initial 10^4 steps, using a bin width 10^{-3}. $a = 1.95$ and $\varepsilon = 0.1$. (a) Single point distribution at $N = 3200$ subtracted by that of $N = 50$. (b) Single point distribution at $N = 3200$ subtracted by that of $N = 200$. See fig. 1b for the distribution itself at $N = 3200$.

ing the scaling of spectra in CML [15]. The Kolmogrov–Sinai (KS) entropy, estimated from the sum of positive Lyapunov exponents, is almost proportional to N within this range of size N. Indeed, the KS entropy per degree of freedom shows very little decrease with size through $N = 50$ to 600 (KS entropy divided by N is 0.3644, 0.3632, 0.3603, and 0.3606 for $N = 50$, 100, 400, and 600, respectively).

Thus the amplification rate of small error (strength of chaotic instability) per degree of

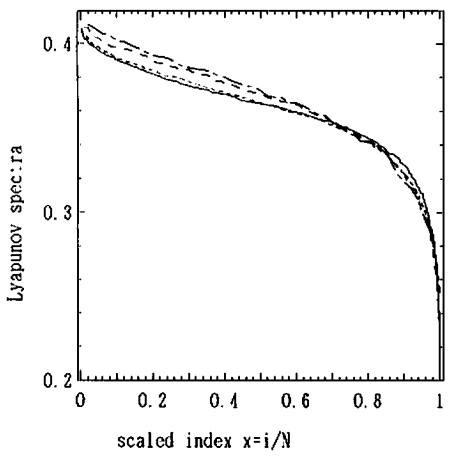

Fig. 11. Scaled Lyapunov spectra for $a = 1.92$ and $\varepsilon = 0.1$. Lyapunov exponents $\lambda(i)$ are plotted as a function of i/N. Spectra are calculated from the product of Jacobi matrices over 2000 time steps after discarding initial 5000 transients. $N = 50$ (dash-dotted line), $N = 100$ (dashed line), $N = 400$ (dotted line), $N = 600$ (solid line).

freedom is almost same for $N > N_c$ and $N < N_c$. However, the way the chaotic instability partitions into modes changes with the increase of N. As is seen in fig. 11, spectra get flatter as N is increased, except for the few top and bottom exponents. Intermediate exponents increase the tendency towards the degeneracy as N is increased up to N_c. Many modes share similar amount of chaotic instability. The above tendency towards flat spectra (degeneracy) is consistent with the emergence of subtle coherence among elements. (Note that the spectra have $(N-1)$-fold degeneracy, when the motion is completely coherent.)

Instability of the fixed point of Perron–Frobenius operator. In the limit of $N \to \infty$, the snapshot distribution $\rho_n(y)$ is defined by the probability that $x(i)$ takes y ($\rho_n(y) \equiv (1/N)\sum_{j=1}^{N} \delta(y - x_n(j))$). If the law of large numbers were valid, the above distribution would be time-independent, and be given by the invariant measure $\rho^*(y)$ for the logistic map $x_{n+1} = (1-\varepsilon)f(x_n) + \varepsilon C$, where C is determined by the self-consistent condition $C = \int \rho^*(y) f(y) \mathrm{d}y$. Our observation of the breakdown of the law of large numbers suggests

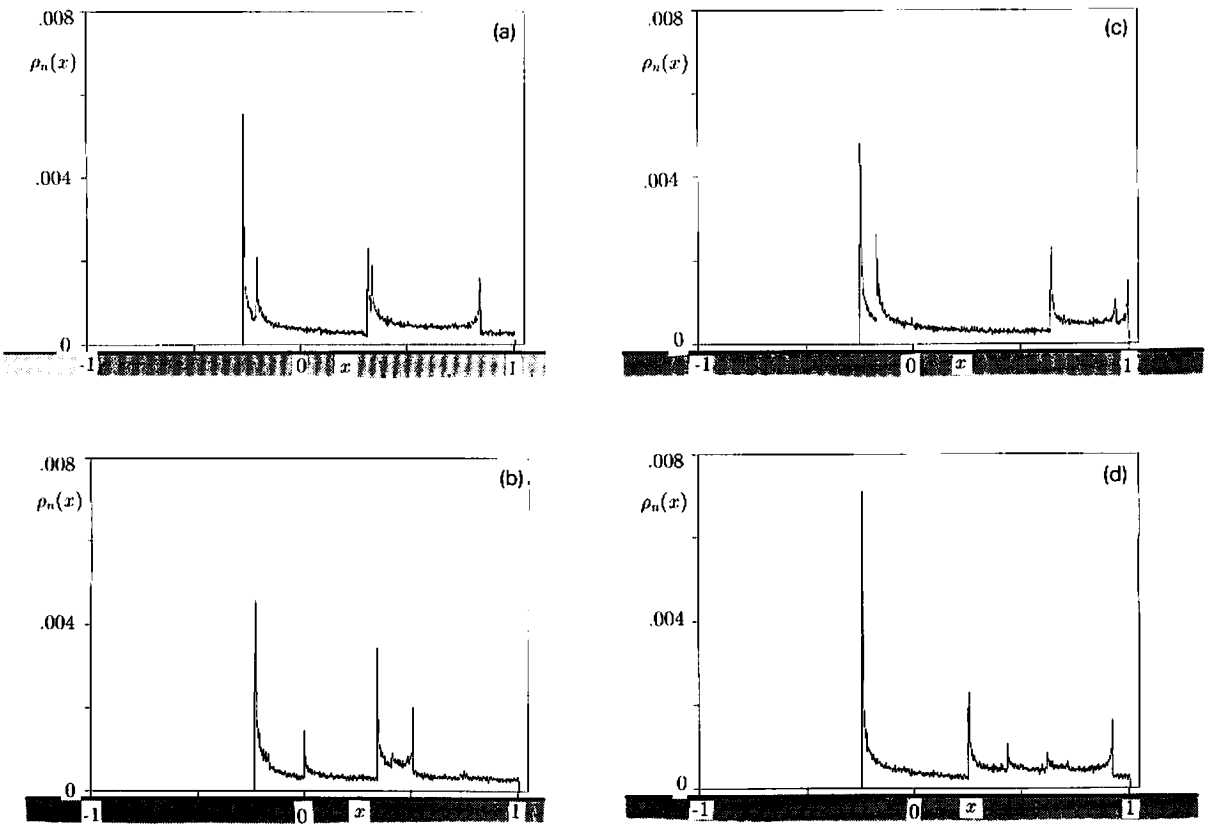

Fig. 12. Snapshot distribution of $x_n(i)$ for our globally coupled logistic map with $a = 1.99$, $\varepsilon = 0.1$, and $N = 10^5$. The distribution is obtained from the data $x_n(i)$ $(i = 1, 2, \ldots, N)$ for a given time step n. The histogram is obtained with the use of the bib size of 2^{-9}. (a) $n = 2005$, (b) $n = 2006$, (c) $n = 2007$, (d) $n = 2008$.

that the above self-consistent probability solution does not exist or is unstable even if it exists. A numerical snapshot for the distribution is given in fig. 12 for $N = 10^5$. Indeed, it is time-dependent.

The single point distribution is calculated with the use of Perron–Frobenius operator [16, 17]. It is written as[#5]

$$\rho_n(x) = \frac{1}{N} \sum_{\text{pre}=+,-} \frac{\rho_{n-1}(y_{\text{pre}})}{|f'(y_{\text{pre}})|}, \tag{4}$$

[#5] If we take a coarse mesh for the integration of eq. (4) (e.g. the order of 0.01), we have often seen approach to a fixed point solution. By increasing the precision of mesh, this solution loses stability. Stability of the fixed point in a coarse-mesh integration may be related with the recovery of law of large numbers in a noisy system in section 4.

where two preimages are given by

$$y_{\text{pre}} = f^{-1}\left(\frac{x - \varepsilon \int f(z)\, \rho_{n-1}(z)\, \mathrm{d}z}{1 - \varepsilon}\right) \tag{5}$$

with two roots of inverse functions $f^{-1}(y) = \pm\sqrt{(1-y)/a}$ for our logistic map. Numerical integration of eq. (4) is given in fig. 13. Although we have tried the integration choosing various initial conditions, the approach to a fixed point function is not observed. This numerical result suggests the instability of a fixed-point solution of eq. (4) or the absence of such solution, as is consistent with the breakdown of the law of large numbers.

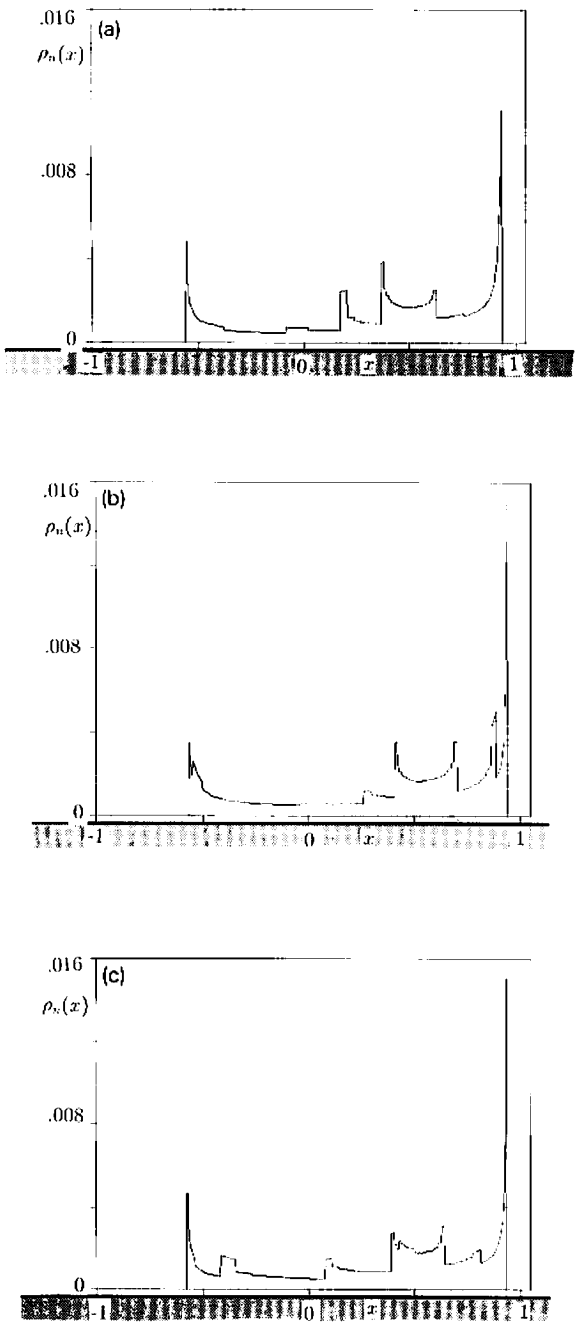

Fig. 13. Snapshot distribution of Perron–Frobenius operator (4) for $a = 1.99$ and $\varepsilon = 0.1$. For the numerical integration of eq. (4), a mesh width 2^{-9} is adopted over the interval of $[-1, 1]$. (a) $n = 160$ (b) $n = 161$ (c) $n = 162$. Even if we wait longer, the approach to a fixed point is not observed (indeed, for a Perron–Frobenius operator, the approach to a fixed point is usually attained within much shorter time steps (e.g., 20 steps)).

4. Destruction of coherence by noise and anomalous fluctuation

With the addition of noise, the above hidden coherence among elements may be destroyed. To study a noise effect, we have simulated a model

$$x_{n+1}(i) = (1-\varepsilon) f(x_n(i)) + \frac{\varepsilon}{N} \sum_{j=1}^{N} f(x_n(j)) + \sigma \eta_n^i,$$

where η_n^i is a white noise generated by an uncorrelated random number homogeneously distributed over $[-1, 1]$. In fig. 14, MSD = $\langle (\delta h)^2 \rangle$ is plotted with the increase of size. If the noise strength σ is larger than a threshold σ_c (≈ 0.005 for the parameters in the figure), the MSD seems to decrease with the size N. The decrease, however, does not obey the expected $1/N$ behavior but has an anomalous dependence on size; $\langle (\delta h)^2 \rangle \propto N^{-\beta}$ with $\beta < 1$[#6].

This anomalous decay is thought to be due to a power law decay of correlation among elements. Assume that mutual correlation between two elements is given by $N^{-\beta}$. Then, the MSD is roughly estimated by[#7]

$$\frac{1}{N^2} \sum_{i,j} \langle \delta h_n(i)\, \delta h_n(j) \rangle = \frac{1}{N} \sum_{j} \langle \delta h_n(1)\, \delta h_n(j) \rangle \approx \frac{1}{N} N^{1-\beta} = N^{-\beta}.$$

Thus it is expected that the mutual information decays with some power in a noisy system if the noise is larger than the threshold mentioned above.

[#6] We cannot deny the possibility that this decrease may again stop with the further increase of size. We have checked MSD only up to $N = 51\,200$ here.

[#7] If no correlation exists, $\langle \delta h_n(i)\, \delta h_n(j) \rangle$ is proportional to the Kronecker $\delta_{i,j}$. If there remains a finite correlation, a finite rate of elements is correlated, which leads to $\langle \delta h_n(1)\, \delta h_n(j) \rangle = cN$. These two limits illustrate the above estimate.

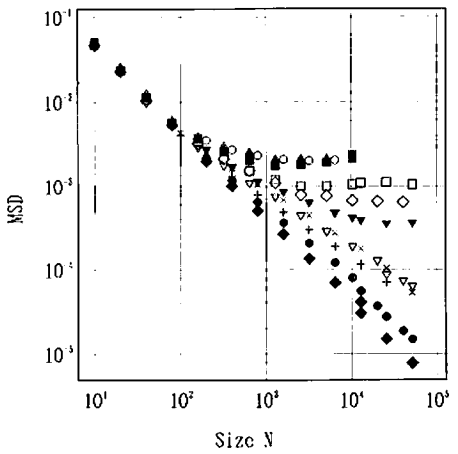

Fig. 14. Mean square deviation of the distribution of mean field h_i in our GCM with the addition of noise. Plotted as a function of system size. $a = 1.99$ and $\varepsilon = 0.1$. The noise strength σ is 0.02 (◆), 0.01 (●), 0.0085 (+), 0.007 (▽), 0.006 (x), 0.005 (▼), 0.0045 (◇), 0.004 (□), 0.002 (■), 0.0008 (▲), 0.0005 (○), and 0.0001 (△) from bottom of top. For $\sigma > \sigma_c \approx 0.005$, MSD decays with $N^{-\beta}$.

In fig. 9, the decay of mutual information is plotted with size. As is expected, it decays as a power function. The power roughly agrees with the above β (fig. 15). The exponent β approaches unity with the increase of σ. $1-\beta$ is plotted as a function of noise σ in fig. 15. Very roughly speaking, $1-\beta$ decays with some power of σ. This power-law dependence still needs an explanation,

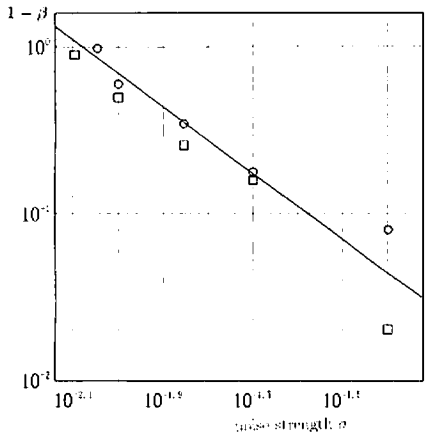

Fig. 15. The exponent $1-\beta$ is plotted as a function of noise strength σ. The exponent β is estimated from fig. 9 (mutual information (□)) and from fig. 14 (MSD (○)).

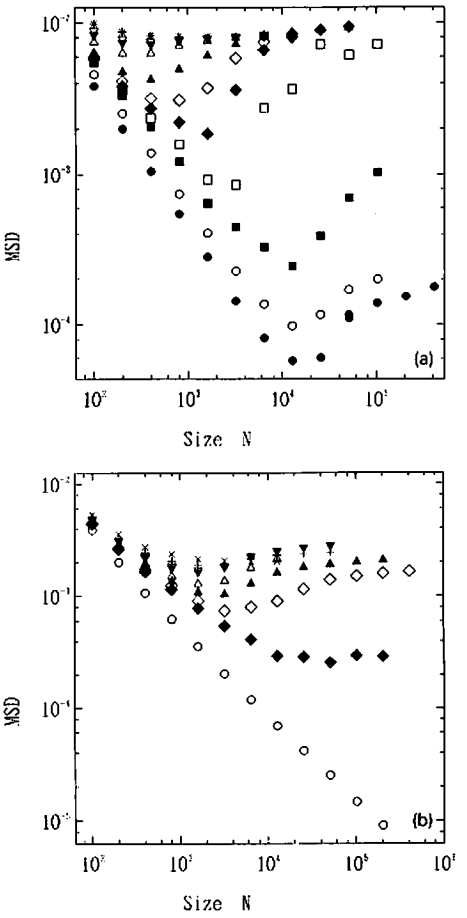

Fig. 16. Mean square deviation of the distribution of mean field h_i for our GCM with inhomogeneous parameters, plotted as a function of system size. $\varepsilon = 0.1$. The distributed parameter $s(i)$ is chosen randomly from the interval $[-\sigma, \sigma]$.

(a) $a = 1.92$. The width σ is 0.05 (●), 0.035 (○), 0.025 (■), 0.024 (□), 0.023 (◆), 0.022 (◇), 0.02 (▲), 0.015 (△), 0.01 (▼), 0.0075 (▽), 0.0005 (x), and 0.00025 (+).

(b) $a = 1.99$. The width σ is 0.02 (○), 0.01 (◆), 0.009 (◇), 0.008 (▲), 0.007 (△), 0.005 (▼), 0.0045 (▽), 0.003 (+), and 0.00025 (x).

which may originate in the hierarchical structure of our attractor [1].

5. Anomalous recovery of coherence in inhomogeneous globally coupled maps

So far we have assumed that all elements are exactly identical. What happens if each element is slightly different? To address this question, we

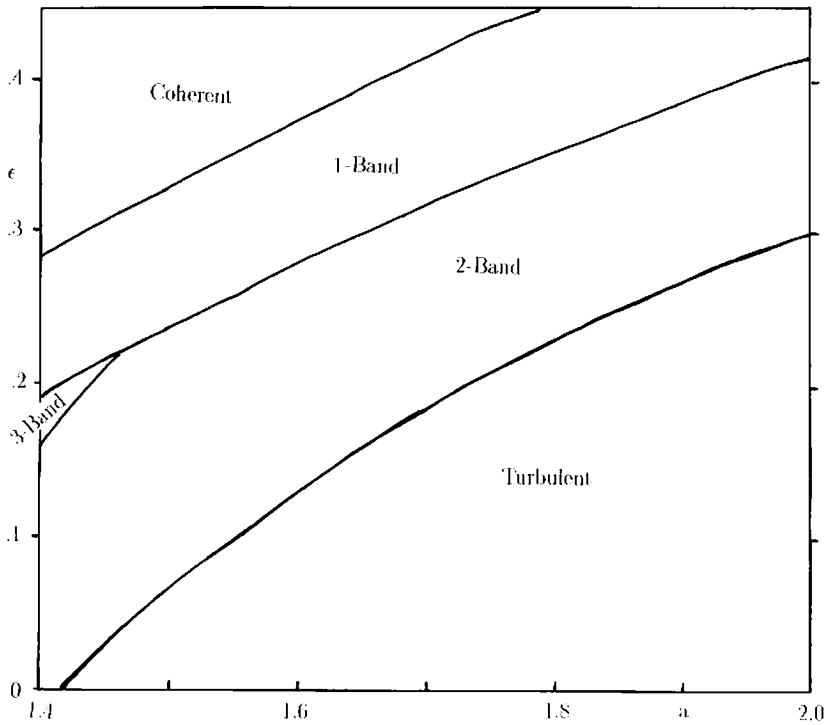

Fig. 17. Rough phase diagram of globally coupled tent map, obtained from the observation of few attractors for each parameter, incremented by 0.01.

choose the following globally coupled map:

$$x_{n+1}(i) = (1-\varepsilon) f^i(x_n(i)) + \frac{\varepsilon}{N} \sum_j f^j(x_n(j)), \tag{6}$$

with

$$f^i(y) = 1 - ay^2 + s(i), \tag{7}$$

where $s(i)$ is a homogeneous random number distributed over $[-\sigma, \sigma]$. Since the map $f^i(y)$ is equivalent to the logistic map with the parameter $a' = a[1 + s(i)]$ by the transformation $y'' = y/[1 + s(i)]$, a larger $s(i)$ leads to a logistic map with a higher peak. Thus the nonlinearity of each map varies by elements.

The above map may be regarded as a model with a static noise $(1-\varepsilon)s(i)$, since the map is written as

$$x_{n+1}(i) = (1-\varepsilon) f(x_n(i)) + (1-\varepsilon)s(i) + \frac{\varepsilon}{N} \sum_j f(x_n(j)) + (1/\sqrt{N}) \times \text{const.}$$

The only difference between this problem and that in section 4 is that the "noise" $s(i)$ here is static, and fixed in time. Since the temporal decorrelation does not seem to be essential to the hidden coherence (see section 3), one might expect that the results are essentially same with the previous section.

In fig. 16, we have plotted the mean square deviation as a function of size. The results are rather intriguing. For a small variance of static noise, there is no significant difference from the

noiseless case. If the variance σ is larger, the mean square deviation $\langle(\delta h)^2\rangle$ again starts to decrease with size as $N^{-\beta}$ with a variable exponent β. What is surprising here is that this decrease continues only up to a size N_c', and that the further increase of size leads to the *increase* of MSD, till it approaches a level close to the noiseless case. Metaphorically speaking, our system behaves as a noisy system up to N_c' and then "notices" that $s(i)$ is not a temporal noise, and goes back to the noiseless case. No further explanation is available so far.

6. Non-universality: globally coupled tent map

To examine the universality of our results, we first study the globally coupled tent map, i.e., eq. (1) with

$$f(x) = a(0.5 - |x - 0.5|). \tag{8}$$

From a linear stability analysis, a coherent state with $x_n(i) = x_n(j)$ is stable if the condition $(1-\varepsilon)a < 1$ is satisfied. Indeed, our system falls on this coherent attractor if this condition is satisfied. There is no clustering state with a small number of clusters if this condition is not satisfied. Since each map is expansive everywhere, it is almost impossible to imagine a mechanism to maintain coherence between two elements. Indeed, none of the elements are synchronized for $(1-\varepsilon)a > 1$.

The phase diagram for the globally coupled tent map is given in fig. 17. As stated above, there is no ordered state with few clusters. Instead, we have band structures in the model.

For a single-band phase, there is strong correlation among elements, although the synchronization is not perfect. The number of clusters is N, but all elements are strongly correlated as is seen in fig. 18a. As the coupling is decreased, the attractor has a two-band structure as in fig. 18b. In a two-band state, elements split into two groups

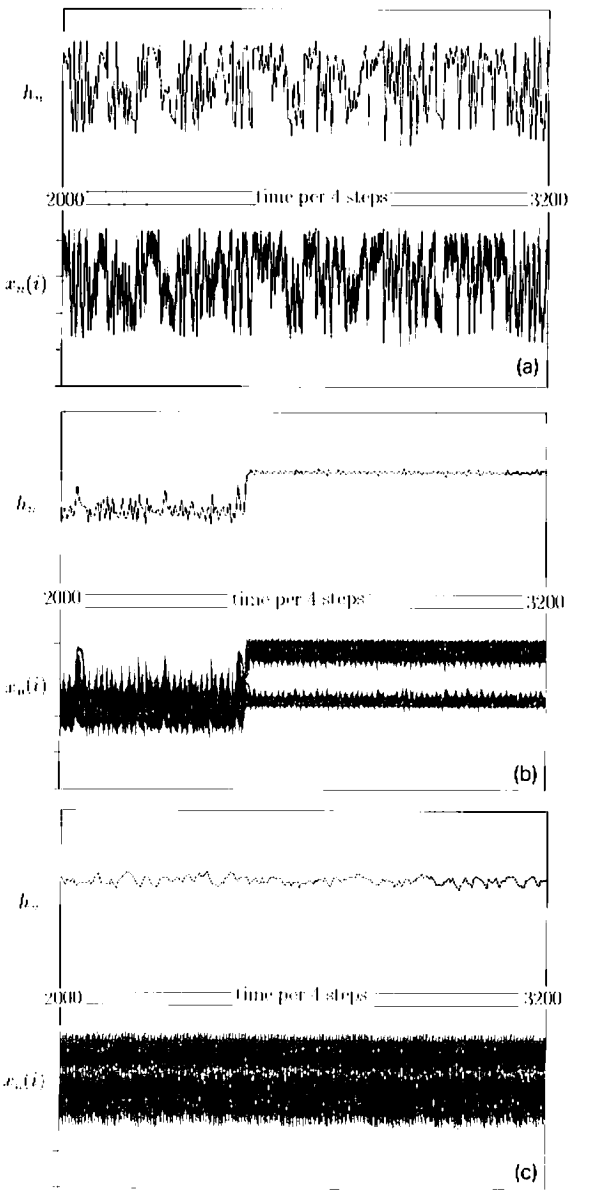

Fig. 18. Time series of $x_n(i)$ (the lower column) and of corresponding mean field h_n (the upper column) of the globally coupled tent map. For the lower column, time series of all elements $x_n(i)$ are overlayed. To remove the oscillation of two-band, they are plotted per 4 time steps. $a = 1.8$, and $N = 100$.

(a) $\varepsilon = 0.4$, for time steps from 2000 to 3200 (a single-band state).

(b) $\varepsilon = 0.3$, for time steps from 2000 to 3200 (after attracted to a two-band state around 2500 time steps, the orbit stays at the two-band forever.)

(c) $\varepsilon = 0.2$, for time steps from 2000 to 320 (a turbulent state).

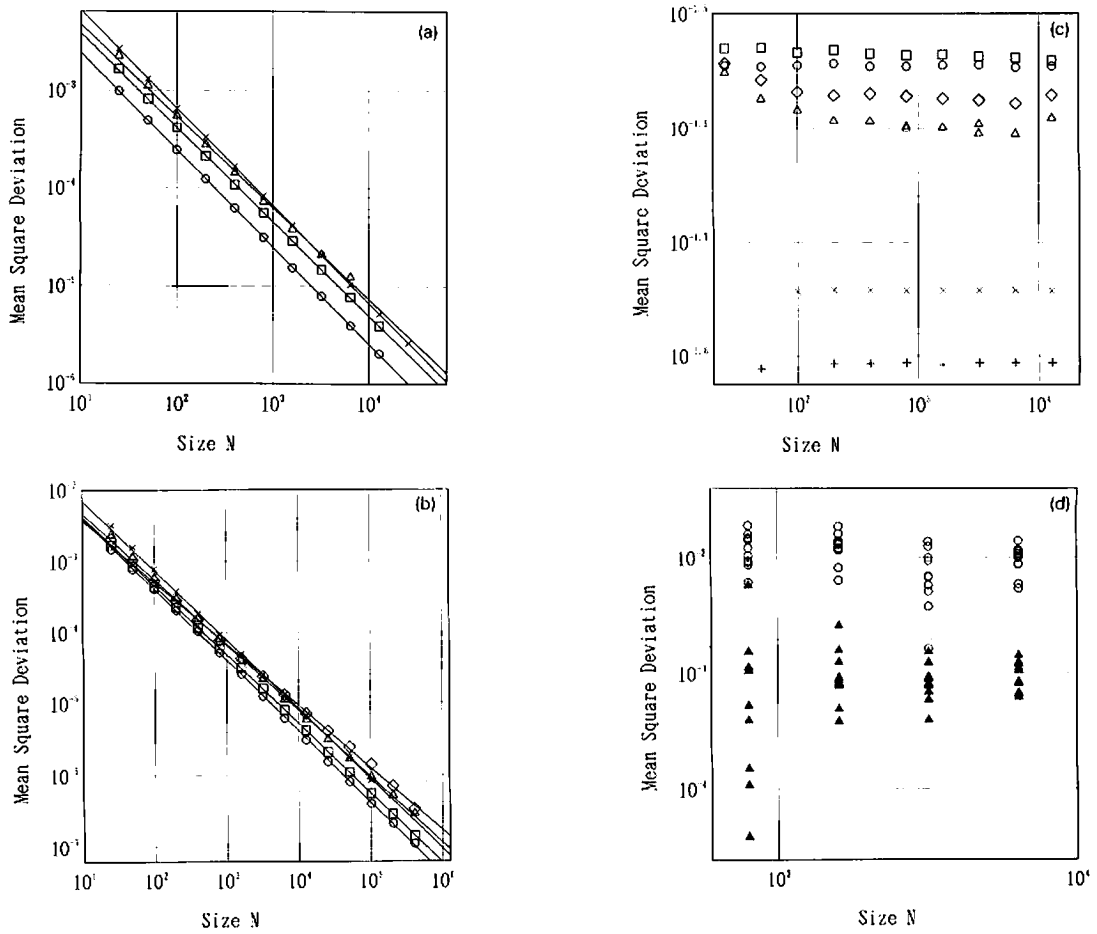

Fig. 19. Mean square deviation (MSD) of the distribution of mean field h for the globally coupled tent map. It is plotted as a function of system size. The MSD is calculated over 10^5 time steps after 10^4 transients.

(a) $\varepsilon = 0.1$. The parameter a is 1.7 (○), 1.8 (□), 1.9 (△), and 2.0 (x).

(b) $\varepsilon = 0.2$. The parameter a is 1.8 (○), 1.85 (□), 1.9 (◇), 1.95 (△), and 2.0 (x).

(c) $a = 1.6$ (+) and $a = 1.65$ (x) for $\varepsilon = 0.3$, while $a = 1.7$ (○), 1.75 (□), 1.8 (◇), and 1.85 (△), for $\varepsilon = 0.4$.

(d) ○ ($a = 1.9$ and $\varepsilon = 0.4$), and △ ($a = 1.9$ and $\varepsilon = 0.3$), from 10 arbitrary chosen initial conditions. At this two band state, different initial conditions can lead to attractors with different partitions to two groups.

with the same oscillation phase of period-two band. In the transition regime between the single- and two-band, we have also observed a state with intermittent switching between the two. With the further decrease of coupling or increase of a, the system enters into a turbulent phase, where no band structure is seen. The elements are perfectly desynchronized (see fig. 18c).

In the turbulent phase, the law of the large numbers and the central limit theorem are valid within our size. So far we have computed MSD up to size 4×10^5, but we have not seen any symptom of deviation from the above theorems within our simulation (see figs. 19a, b) for MSD and fig. 20a for the distribution). Numerical integration of Perron–Frobenius operator (see eq. (4)) leads to a fixed-point solution, as is consistent with the disappearance of the mean field fluctuation at $N \to \infty$. This result is in strong contrast with that for a globally coupled logistic map.

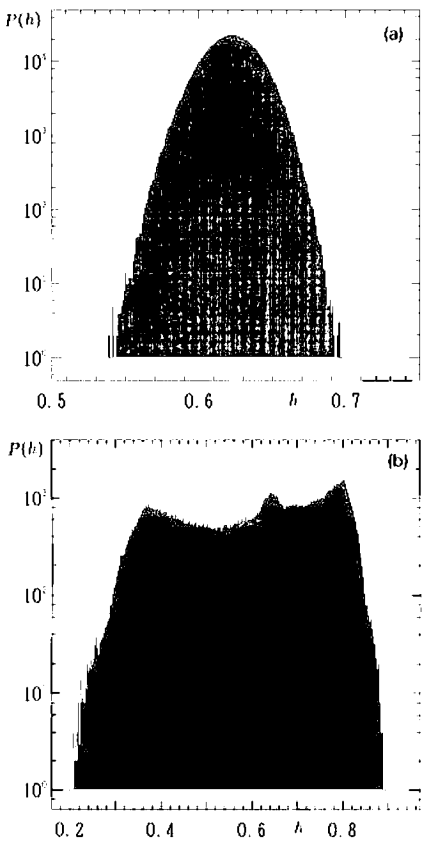

Fig. 20. Semi-log plot of histogram of mean field h_n for the globally coupled tent map. Sampled over 10^5 time steps, after discarding the initial 10^4 steps, using the bin width 10^{-3}. (a) $a = 1.95$, $\varepsilon = 0.1$, and $N = 200$ (b) $a = 1.87$, $\varepsilon = 0.4$, and $N = 3200$.

On the other hand, the law of large numbers is completely broken in the single-band phase, since motion of elements is strongly correlated. MSD does not show any decrease with the size at all (see fig. 19c). The distribution of mean field is far from Gaussian. The origin of this discrepancy is ascribed to low-dimensional chaos. For low-dimensional chaos, the invariant measure is far from Gaussian, as is well known. Since all elements are "slaved" by this low-dimensional motion there is neither a decrease of mean square deviation of the distribution nor an approach to Guassian form.

In the two-band state, there are many attractors depending on the partition of elements into two groups. Besides this dependence on initial condition, the MSD does not decrease with N at all. The dependence of MSD on initial condition looks decreased since the partition to two groups has smaller variance as N is increased.

7. Mean field fluctuation in circle maps

As another class of globally coupled dynamical systems, we have investigated the globally coupled circle map

$$x_{n+1}(i) = x_n + \frac{K}{2\pi}\sin(2\pi x_n(i)) + \Omega + \frac{\varepsilon}{2\pi N}\sum_j \sin(2\pi x_n(j)). \qquad (9)$$

which is thought to belong to the same class with globally coupled oscillators (see ref. [4]). Again the map shows coherent, ordered, partially ordered, and turbulent phases as well as a quasiperiodic state [3]. In fig. 21, we have again plotted the size dependence of the MSD $\langle(\delta h)^2\rangle$ of the mean field $h_n = (1/N)\Sigma_j \sin(2\pi x_n(j))$, for quasiperiodic and turbulent states.

We note that the mean field fluctuation does not violate the law of large numbers for a quasiperiodic state. As is seen in fig. 21a, MSD approaches zero very quickly. Here the MSD $\langle(\delta h)^2\rangle$ depends on initial conditions, since the initial information on phase is not lost. The ordering of phases of elements is conserved through the dynamics [4]. Since MSD vanishes at $N \to \infty$, the dynamics of our coupled system approaches a degenerate high-dimensional torus, given by N independent circle maps.

In the turbulent state, MSD decreases up to some crossover size N_c and then remains finite against the further increase of size (see fig. 21b). The behavior belongs to the same class as globally coupled logistic map.

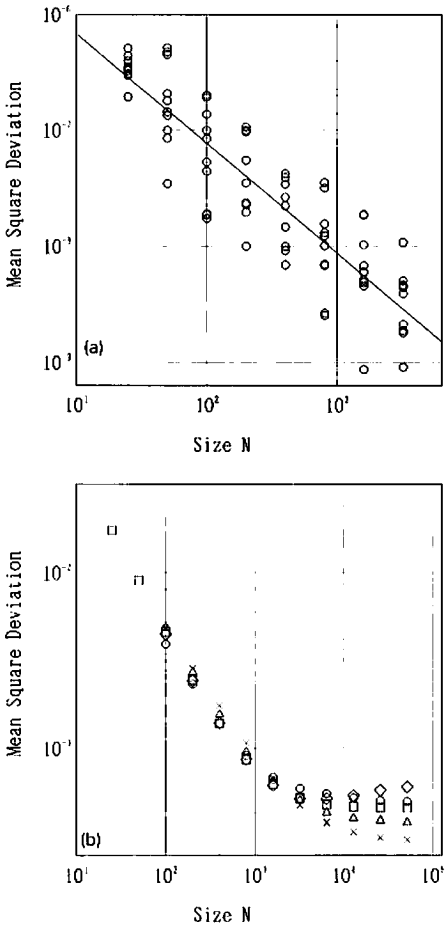

Fig. 21. Variance of the mean field $h_n = (1/N) \times \Sigma_j \sin(2\pi x_n(j))$ for the globally coupled circle map (9). The variance $\langle (h - \langle h \rangle)^2 \rangle$ is plotted with size N, calculated from 10000 temporal steps after discarding 3000 transient steps starting from a random initial condition. $\varepsilon = 0.2$ and $\Omega = 0.3$. (a) MSD from 10 randomly chosen initial conditions for $K = 0.5$ (degenerate torus states). (b) $K = 1.4$ (○), $K = 1.5$ (□), $K = 1.6$ (◇), $K = 1.65$ (△), and $K = 1.7$ (×).

8. Summary and discussion

We have investigated the distribution of mean field in a turbulent state for globally coupled maps. For logistic and circle maps, finite fluctuation remains even in the limit of $N \to \infty$, implying the breakdown of the law of large numbers.

Heuristically we can summarize our results for globally coupled logistic maps as follows: (1) Up to a crossover size N_c, the mean square deviation decreases as $1/N$, but then stays constant with a further increase of size. (2) Up to $N < N_c$ the mean field distribution approaches a Gaussian form, but there remains a slight deviation from its form for a larger size. (3) The remaining MSD is roughly proportional to $1/N_c$, which has a non-monotonic and large dependence on the nonlinearity. (4) As the crossover size $N < N_c$ is larger, the deviation from Gaussian form gets smaller. (5) MSD and $1/N_c$ decrease with the coupling ε roughly as ε^2.

The remaining fluctuation implies the appearance of hidden coherence among elements. Existence of finite correlation among elements is confirmed by finite mutual information. Lyapunov spectra for the map also show the tendency towards coherence with the increase of size. If the mean field fluctuates in the limit of $N \to \infty$, the single-point (snapshot) distribution is also time-dependent, and deviates from the invariant measure for a logistic map. Indeed, numerical integration of the Perron–Frobenius operator suggests the instability of self-consistent (fixed-point) solution for the measure.

When a large enough noise is added to our system, the law of large numbers is recovered, but the decrease of variance obeys the form of $N^{-\beta}$. Here the exponent β is dependent on the noise strength. The mutual information also decays with this power, implying the destruction of hidden coherence by noise. We have to note that the mean-field fluctuation *decreases* drastically with the addition of noise, although it looks rather paradoxical.

As a related problem, we have studied our system with the addition of a "static noise"; in other words, a globally coupled map with inhomogeneous parameters. The variance of mean field fluctuation again decreases with some power up to some size, but then increases back to an original noiseless level with the further increase of size. This remarkable behavior suggests that inhomogeneity among elements can partially destroy the hidden coherence for a small size, but the coherence re-appears for a larger size.

Two other globally coupled maps are studied: tent maps and circle maps. In a globally coupled tent map, the mean field fluctuation satisfies the law of large numbers in the turbulent phase, while the fluctuation remains finite even for $N \to \infty$ in the phase in the circle map. These results suggest that the breakdown of the law of large numbers is generally seen in a turbulent state with local stretching and contraction. As N is increased, the contraction effect brings about hidden coherence among elements, leading to a crossover to constant remaining fluctuation for a larger size. A slight change of single-point distribution (and Lyapunov spectra) seems to support the enhancement of contraction effect with the size increase. If the map includes only the stretching, such coherence cannot be created with the size increase, implying the satisfaction of the condition for the law of large numbers, as is verified in the globally coupled tent map.

If the above argument is correct, we expect that the breakdown of the law of large numbers is universal among globally coupled dynamical systems with local contraction and stretching. If this is the case, we may have a novel viewpoint on a macroscopic fluctuation in various fields: Does the average activity of neural field satisfy the law of large numbers and central limit theorem? Is the distribution of mean velocity field Gaussian in turbulence? Does the mean force field in galaxy, protein dynamics, and in an ensemble of vortices obey the law of large numbers? We believe that all of these questions will be answered in the negative due to the hidden coherence in globally coupled chaos. In particular, it is an interesting question if the number of neurons is larger than the crossover size discussed in the present paper. One of the reasons for the huge number of neurons may be to create the hidden coherence.

The mechanism of the origin of the hidden coherence is not yet clarified, although the observed, slight tendency to increase the contraction effect with size may be essential to the creation of the coherence. It will be important to construct thermodynamic formalism with the use of Perron–Frobenius operator [18] or with the extension of statistical mechanical formalism on CML[#8]. Once such theoretical formalism is constructed, it may reveal the origin of hidden coherence.

The breakdown of the law of large numbers is characteristic of globally coupled chaos. Neither a pure noise nor a quasiperiodic state (see section 7) breaks the law. Chaos has two faces, order and randomness: both are necessary to create the hidden coherence with the increase of the number of elements. In this respect, the late professor Kazuhisa Tomita has correctly adopted the term "coherent irregularity" for chaos [20].

Acknowledgement

I would like to thank K. Ikeda, I. Tsuda, Y. Takahashi, T. Konishi, K. Nemoto and T. Ikegami for useful discussions, and H. Tasaki for critical comments. I would also like to thank National Institute for Fusion Study at Nagoya for the computational facility of FACOM M380 and VP200. This work is partially supported by Grant-in-Aid for Scientific Research from the Ministry of Education, Science, and Culture of Japan.

References

[1] K. Kaneko, Phys. Rev. Lett. 63 (1989) 219; Physica D41 (1990) 38; Phys. Rev. Lett. 65 (1990) 1391; 64 (1991) 243 (E).
[2] K. Kaneko, J. Phys. A 24 (1991) 2107.
[3] K. Kaneko, Globally coupled circle maps, Physica D 54 (1991) 5.
[4] P. Hadley and K. Wiesenfeld, Phys. Rev. Lett. 62 (1989) 1335.
[5] K. Wiesenfeld et al., Phys. Rev. Lett. 65 (1990) 1749; H.G. Winful and L. Rahman, Phys. Rev. Lett. 65 (1990) 1575.
[6] C. Bracikowski and R. Roy, Chaos 1 (1991) 49.
[7] M. Eigen and P. Schuster, The Hypercycle (Springer, Berlin, 1979);

[#8] See ref. [19] for thermodynamic approaches to CMLs.

T. Ikegami and K. Kaneko, Phys. Rev. Lett. 65 (1990) 3352;
K. Kaneko and T. Ikegami, submitted to Physica D (1991).
[8] See, e.g., W. Freeman, Brain Res. Rev. 11 (1986) 259.
[9] K. Kaneko, Prog. Theor. Phys. 72 (1984) 480; 74 (1985) 1033; Collapse of Tori and Genesis of Chaos in Dissipative Systems (World Scientific, Singapore, 1986); Physica D 34 (1989) 1; D 37 (1989) 60 and references therein.
[10] J.P. Crutchfield and K. Kaneko, in: Directions in Chaos (World Scientific, Singapore, 1987).
[11] K. Kaneko, Phys. Lett. A149 (1990) 105.
[12] R. Shaw, Z. Naturforsch. 36 a (1981) 80.
[13] K. Kaneko, Physica D 23 (1986) 436;
K. Ikeda and K. Matsumoto, Phys. Rev. Lett. 62 (1989) 2265.
[14] M. Mezard, G. Parisi and M.A. Virasoro eds., Spin Glass Theory and Beyond (World Scientific, Singapore, 1987).
[15] K. Kaneko, Physica D 23 (1986) 436.
[16] R. Bowen and D. Ruelle, Invent. Math. 29 (1975) 181;
D. Ruelle, Thermodynamic Formalism (Addison-Wesley, Reading, MA, 1978).
[17] Y. Oono and Y. Takahashi, Prog. Theor. Phys. 63 (1980) 1804.
[18] K. Kaneko, Phys. Lett. A 139 (1989) 47;
J.M. Houlerik, I. Webman and M.H. Jensen, Phys. Rev. A 41 (1990) 4210.
[19] L.A. Bunimovich and Ya.G. Sinai, Nonlinearity 1 (1989) 491;
K. Kaneko, Prog. Theor. Phys. Suppl. 99 (1989) 263.
[20] K. Tomita, Prog. Theor. Phys. Suppl. 79 (1984) 1.